Dip-coating deposition of nanocomposite thin films based on water-soluble polymer and silica nanoparticles

Syrine Jebali, Marylène Vayer, Khaled Belal, Frédéric Mahut, Christophe Sinturel

Dip-coating deposition of nanocomposite thin films based on water-soluble polymer and silica nanoparticles

Syrine JEBALI[1], Marylène VAYER[1], Khaled BELAL[2], Frédéric MAHUT[3], Christophe SINTUREL[1]*

[1] Interfaces, Confinement, Matériaux et Nanostructures (ICMN), CNRS-Université d'Orléans, UMR 7374, 1B Rue de la Férollerie, C.S. 40059, 45071 Orléans Cedex 2, France

[2] Kemica Coatings, Za du Bois Gueslin, 28630 Mignières, France

[3] Centre de Nanosciences et de Nanotechnologies (C2N), CNRS-Université Paris Saclay, UMR 9001, 10 Boulevard Thomas Gobert, 91120 Palaiseau, France

*corresponding author: christophe.sinturel@univ-orleans.fr

Keywords: water-soluble polymer, dip-coating, nanocomposite thin films, silica nanoparticles

Highlights:

- PVP thin films loaded with silica nanoparticles were prepared by dip-coating.
- Thicknesses of the films are not affected by the presence of nanoparticles.
- Nanoparticles are incorporated over the whole range of withdrawal speeds.
- The deposition regime does not influence the nanoparticle concentration in the film.
- Unexpected nanoparticle surface depletion is observed in the capillary branch.

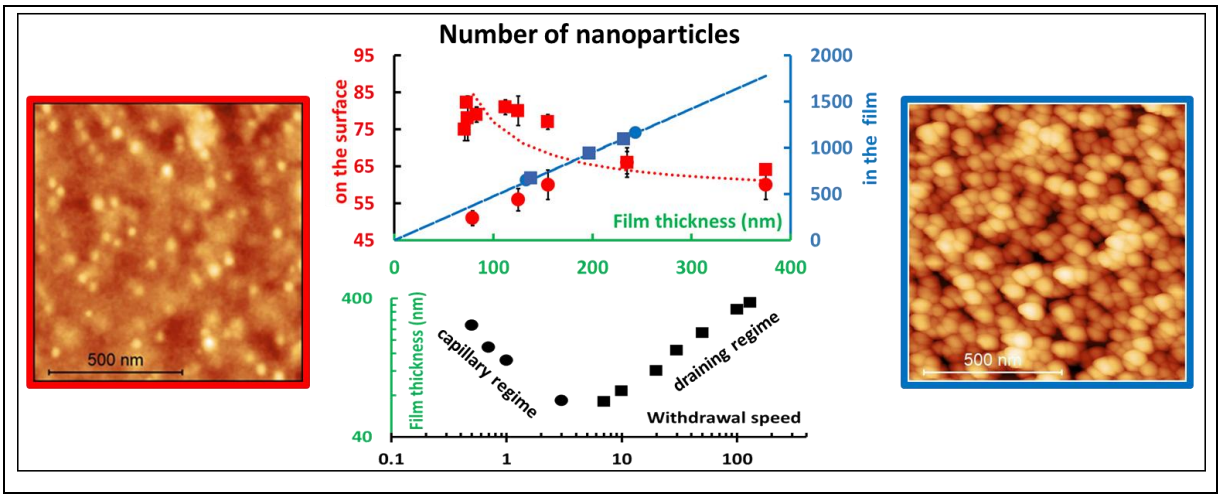

Abstract

Dip-coating deposition of nanocomposite thin films composed of polyvinylpyrrolidone and silica nanoparticles was studied using atomic force microscopy and scanning electron microscopy. The presence of particles (up to 5wt. %) did not modify the film thickness, which followed a classical additive law of an evaporative regime and a draining regime. Within film volume, no preferential retrieval of particles nor polymer occurred during deposition. This was consistent with the size of particles small enough so that particles were not trapped in the meniscus. For the thicker films prepared in pure capillary and draining regimes, the number of particles observed on the surface was independent of the thickness and was in full agreement with a homogenous distribution of the particles in the film. In contrast, for the thinner films (near the critical withdrawal speed) the number of particles differed in the two regimes. In the draining branch, the number followed the theoretical prediction with an increased number of particles as the thickness decreases, due to the presence of an exclusion zone at the interfaces. Unexpectedly, in the capillary branch, a depletion of particles was observed and could result from competition and interplay between time-dependent phenomena that took place during the dip-coating. This behavior will need to be carefully considered when preparing nanocomposite thin films where surface properties such as roughness or wettability need to be considered.

Introduction:

Dip-coating is a widely-used technique which consists in dipping a substrate in a liquid and removing it at a controlled withdrawal speed.[1,2] The technique is applied for industrial coating purposes but is also extensively studied from an academic point of view.[1] Several behaviors have been experimentally observed, theoretically studied and applied as a function of the liquid (type and composition), substrate (form and nature, structure, surface wetting) [3, 4, 5, 6] withdrawal speed and environment.[2] Two categories of cases can be distinguished, depending on whether the liquid is evaporative or not.

In the non-evaporative liquid category, dip-coating results in liquid film. The simplest case is that of a non-evaporative Newtonian liquid described by the Landau-Levitch model.[7] In this case, the thickness of the liquid film increases with the withdrawal speed due to the competition between the viscous drag and the surface tension at the meniscus. Within this category of non-evaporative liquid, the case of two immiscible liquids[8] and of particles in suspension in a non-evaporative liquid[9, 10, 11, 12, 13, 14,] have been studied and described. In the case of particles in suspension in a non-evaporative liquid, dip-coating can result in a liquid film with or without particles depending on the size of the particles. It has been shown that there is a critical particle size above which the particles remain in suspension. This property has been used to separate particles and to sort them by size in a suspension[9,10.]

The other category concerns an evaporative liquid, where dip-coating results in a dried thin film composed of the solid fraction present in the suspension. In this case, two regimes are generally observed depending on the withdrawal speed. At low speed, a capillary regime is observed with an increase in the thickness of the film with the decrease in speed. At high speed, the draining regime is observed with an increase in the thickness of the film with the speed.[15] These two regimes have been evidenced and studied in many systems, from particles in suspension in an evaporative liquid[16, 17, 18] to sol-gel inorganic systems,[2, 19] polymeric films[20, 21, 22, 23] to polymer nanocomposites with inorganic nanoparticles (NPs) within a non-newtonian fluid.[24]

In the polymer field, this technique has been applied to control the morphology of amorphous polymer blends[22], the crystallization of polymers[25], to organize particle monolayers on a surface[26] or to prepare polymer nanocomposites with nanoparticles.[23, 27, 28]

In the case of polymeric nanocomposites composed of polymer and nanoparticles, Kumar and coworkers[29] pointed out the importance of fully describing the nanocomposites, i.e. the structure of dispersion and the spatial distribution of the NPs in the polymer matrix, the

existence of a polymer layer at one interface and its role, the dynamics in polymer nanocomposites… The control of the nanocomposite depends strongly on the processing method used to prepare the nanocomposites. For processes driven by solvents, the role of solvent evaporation in polymer and NP distributions plays a great role.[30]

In this paper, we study such a process (dip-coating of an NP/polymer suspension in ethanol/water) and describe the resulting nanocomposite thin film, focusing on the volumic ratio of NPs/polymer in the dry film compared to the volumic ratio in the suspension, and the distribution of the NPs in the polymeric matrix. The objective of this work was to examine the potential effect of the deposition regime (involving different physical processes) on the retrieval of the components of the suspension, paying particular attention to the situation at the surface of the film, which drives effects such as roughness and wettability. The chosen system was a suspension of polyvinylpyrrolidone (PVP) and silica Ludox AS nanoparticles (NPs). PVP is a widely recognized polymer with a long history of use in various applications, owing to its exceptional solubility in both water and organic solvents and can be easily cross-linked. This characteristic makes it an ideal candidate for controlling the dispersion and stabilization of nanoparticles during thin film deposition processes. Furthermore, PVP exhibits excellent film-forming properties, allowing to create uniform and stable thin films with controlled nanoparticle distributions. Its ability to adsorb onto the surface of nanoparticles and provide steric stabilization enhances capability to engineer the film's structure and properties. Moreover, PVP is known for its biocompatibility and non-toxic nature, making it particularly used for applications in areas such as biomedicine and nanotechnology. The chosen particles are water stabilized, nanometric, costless, monodispersed silica particles, which can be easily post-functionalized for further applications.

Material and methods

Materials

1-ethenylpyrrolidin-2-one (polyvinylpyrrolidone (PVP)) Mw= 58 kg mol^{-1} from Alfa-Aesar and Ludox®AS-40 colloidal silica NPs (40 wt. % SiO_2 suspension stabilized with ammonium in water) suspension from Sigma–Aldrich were used as received.

Polymer solution and nanocomposite suspension preparation

To prepare the polymer solution and the nanocomposite suspensions, ethanol was chosen as solvent rather than water since ethanol is more volatile and thus gives a better quality film.

A PVP solution (50 mg ml^{-1}) was prepared by mixing the polymer and ethanol at room temperature, under magnetic stirring for 1h. This solution will be named A0 hereafter.

For the nanocomposite suspensions, a diluted suspension of silica nanoparticles (NPs) in water (NP 20 wt. %) was first prepared from the commercial Ludox AS-40 suspension. A given amount of this suspension was then dispersed in ethanol before adding a weighed amount of PVP in order to get a suspension at 50 mg ml^{-1} in ethanol of PVP, with a known weight ratio between NP and PVP in the dried films of 1, 5 and 10 (weight NP/PVP ratio). As an illustration, to prepare 15 ml of PVP/NP solution (50 mg ml^{-1}) having an NP/PVP weight ratio of 10:100 (A10), 375 mg of the colloidal suspension of Si NP (NP 20 wt. %) was dispersed in 11.5 g of ethanol before adding 750 mg of PVP. The suspension was then stirred during at least 1 h. A transparent suspension with no evidence of sedimentation or aggregation was obtained and was used the same day.

Four compositions named A0, A1, A5, and A10 were prepared with weight proportions between NP and PVP in the dried films of 0:100, 1:100, 5:100 and 10:100. The compositions are presented in table 1. All the concentrations of the stock materials were determined and taken into account (see SI-1).

	A0	A1	A5	A10
nominal NP: PVP wt. ratio	0:100	1:100	5:100	10:100
%vol. of PVP+NP (ml ml^{-1}) in suspension	3.83	3.82	3.78	3.74
conc. of PVP+NP (g cm^{-3}) in suspension	0.046	0.046	0.048	0.050
% vol. of NP (ml ml^{-1}) in the dry film	0	0.46	2.24	4.39

table 1: characteristics of the prepared suspensions A0, A1, A5 and A10

Dynamic light scattering experiment

To determine the distribution of the size of nanoparticles in suspension, dynamic light scattering (DLS) measurements were performed on the suspension with a Zetasizer Nano ZS90 (Malvern Panalytical) on the Ludox suspension in ethanol and also on the A10 suspension used for the dip-coating experiment. The suspension was diluted with deionized water or ethanol to adjust the light strength to the measurement condition.

Dip coating film deposition

Thin films of polymer nanocomposites were prepared at room temperature on a silicon substrate by dip-coating (dip-coater QPI-168, Qualitech Industrial Products, India). The substrates (10 mm * 70 mm) were first cleaned using acetone and ethanol. The same recipient (diameter = 2.5 mm, total height= 57 mm) and the same volume of suspension (15 ml) was always used in order to keep the deposition conditions constant.

A 30 mm long section of the substrate was immersed, left for 1 min and withdrawn at a speed from 0.3 to 700 mm min^{-1}. After complete evaporation of the ethanol, dried nanocomposite thin films on silicon were obtained.

Ellipsometric spectroscopy measurement

The thickness of the films was estimated using ellipsometric spectroscopy. The measurements were performed on a M-2000 Auto-angle ESM-300 base ellipsometer from Woollam (spectral range 400–830 nm). Data were fitted with the software from the ellipsometer using a Cauchy model. The measurements were always performed within the same region of the substrate (region of interest, ROI) located on a line in the middle of the width of the sample, between 15 mm and 20 mm from the bottom of the sample (the part of the sample that emerges last) to ensure reproducibility. Thank to thorough thickness measurements at various points across the ROI, we verified that the thickness variation was minimal in the considered zone. The given value is an average thickness value using at least five thickness measurements. All subsequent analyses (SEM and AFM) were carried out on the same ROI, ensuring that the same volume was analyzed with the different characterization techniques.

Scanning Electron Microscopy

A scanning electron microscope Thermofisher Scientific – Magellan-400L in low vacuum mode, with a beam energy at 15 keV was used to obtain images of the surface of nanocomposite thin films containing NPs with magnification from 150 000 to 250 000. All the images were recorded with the secondary electron in-lens TLD detector. This detector collects mainly secondary electrons, with a small contribution of backscattered electrons. No prior metallization of the samples was needed before imaging.

The top-view images were used to count the NPs in the surface layer of the film.

After a cryo-fracture of the sample in N_2-liquid, images of the cross-section of the nanocomposite thin film were recorded. They were used to visualize the location of NPs in the thickness of the nanocomposite thin film, to count the NPs in the film and to determine the thickness of the film.

Transmission Electron Microscopy

Transmission Electron Microscopy (TEM) was used to visualize the NPs shape and size dispersed in water, ethanol and after adding the polymer. A drop of each suspension was deposited on a copper TEM grid and left to dry. TEM characterizations were carried out using a Philips CM20 instrument operated at an accelerating voltage of 200 kV.

Atomic Force Microscopy

Atomic Force Microscopy (AFM) was used to examine the surface topography of the film, to quantify the NPs on the surface and in the volume of the nanocomposite film, and to determine the film thickness. AFM imaging was performed in air at room temperature in tapping mode on an AFM Dimension Icon with ScanAsyst from Bruker, USA with TESPA-300 silicon cantilevers (resonance frequency 320 kHz, spring constant: 40 N m^{-1}). All the AFM images displayed are height images, 1 × 1 μm².

- *Quantification of the NPs on the surface:*

At least five 1 × 1 μm² and 512 * 512 pixel images on three different samples for each condition (composition of the suspension, withdrawal speed) were recorded at different locations in the ROI to check the uniformity of the surface and the reproducibility of the deposition. Image analysis was performed using Gwyddion and Image J software in order to quantify the NPs present on the surface. The standard deviation was calculated over the counted numbers of nanoparticles (NPs) for all AFM images captured within the ROI and for each specific experimental condition.

- *Quantification of the NPs in the film:*

To estimate the total number of NPs in the polymer films, the films were calcined at 740 °C during 1h. These conditions ensure a complete degradation of the organic compounds.[31] AFM imaging of these calcined films was carried out and the number of NPs left on the surface after calcination was quantified by counting with Image J software.

- *Thickness determination of the films:*

The thicknesses of the films were determined by AFM imaging of a scratch, deliberately made with a needle on the film. Thicknesses determined using AFM were in very good agreement with the ones determined using ellipsometric spectroscopy.

Results and discussion

1-Characterization of the NPs in suspension

To measure the NPs size distribution and to check their stability in the suspension, DLS analysis was carried out. DLS spectra of NPs dispersed in ethanol and in the A10 suspension are shown in Figure SI-2. The two samples presented a uniform distribution of hydrodynamic NP diameter, indicating the good stability of the NPs in the suspensions with no aggregation, even in the presence of the polymer. The average diameter of NPs in ethanol and A10 suspension were 37.8 ± 3.5 nm and 68.1 ± 4.0 nm, respectively. The average particle size of NPs in the A10 suspension was significantly larger due to the encapsulating of NPs by the polymeric matrix. PVP is well known to act as a surface stabilizer and a nanoparticle dispersant, which tends to establish bonds with NPs, thus increasing the Si nanoparticle size[32].

TEM characterization was also performed in order to determine the shape and quantify the size of the NPs dispersed in ethanol. It confirmed the good dispersion of the NPs, which had a size of 26.0 ± 1.9 nm (Figure SI-3a).

2- Thickness of the film as a function of the withdrawal speed.

Figure 1 shows the variation of the film thickness (after drying) as a function of the withdrawal speed for the neat PVP solution (A0) and the nanocomposite A1, A5, and A10 suspensions, deposited by dip-coating for withdrawal speeds between 0.3 and 130 mm min^{-1}. This range of speeds, which covers the two deposition regimes, was chosen in order to obtain high quality homogeneous films with a good coverage of the substrates.[16]

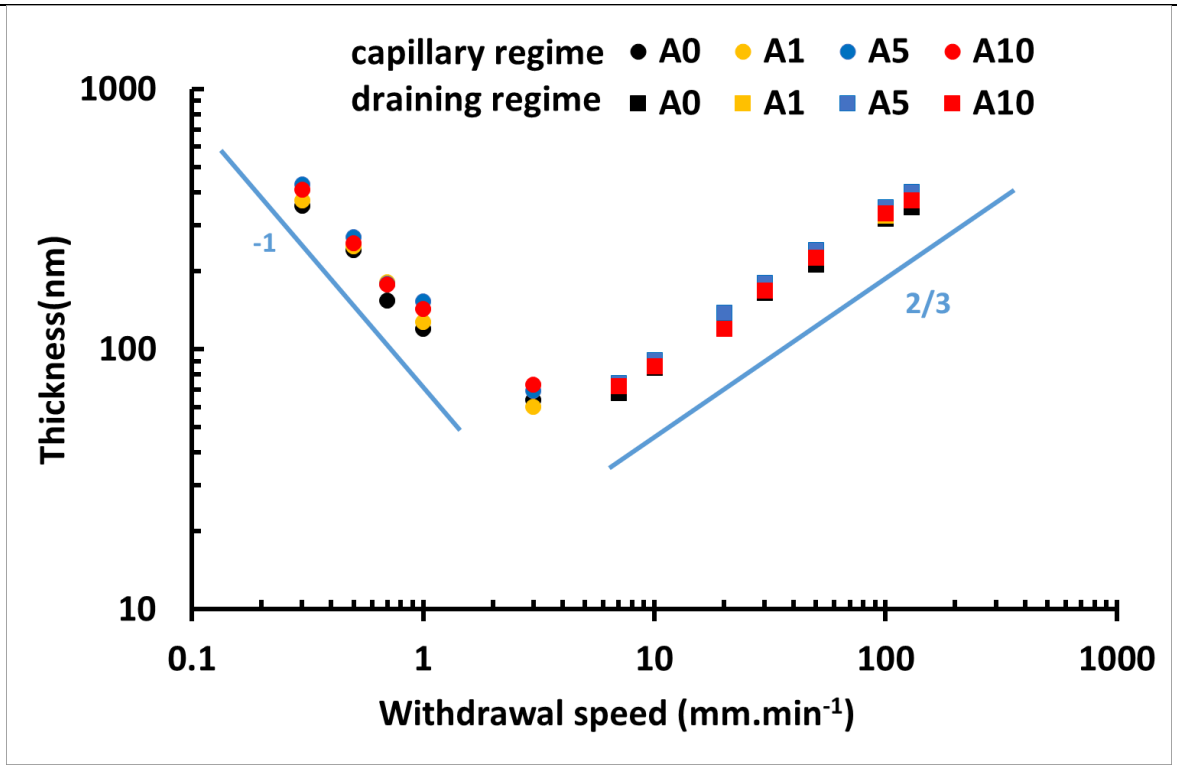

Figure 1: Film thickness as a function of the withdrawal speed in log/log scale for the polymer solution A0 and the nanocomposite suspensions A1, A5 and A10 in the deposition draining (square) and capillary (circle) regimes. Lines with slopes -1 and 2/3 are drawn to guide the eyes. The error bars (relative standard deviations less than 2%) are not represented.

In a log/log scale, the curves for all the compositions (A0 up to A10) are superposed, indicating that the presence of the NPs in the suspension does not modify the deposition regime. The thickness versus the withdrawal speed exhibits a typical "V" shaped curve. It first decreases linearly with increasing speed, goes through a minimal thickness for a critical speed, and then increases linearly for higher speeds. For all the compositions, the critical speed ranges between 2 and 10 mm min^{-1} and a minimum thickness between 60 and 90 nm.

suspension name	slope in the capillary regime	slope in the draining regime	E evaporation rate	D global draining constant
A0	-0.97 ± 0.02	0.53 ± 0.01	6 ±1 x 10^{-13}	2.1 ± 0.5 x 10^{-4}
A1	-0.99 ± 0.02	0.57 ± 0.01	5 ± 1 x 10^{-13}	2.2 ± 0.5 x 10^{-4}
A5	-1.02 ± 0.02	0.56 ± 0.01	3 ±1 x 10^{-13}	2.8 ± 0.5 x 10^{-4}
A10	-0.99 ± 0.02	0.58 ± 0.01	5 ±1 x 10^{-13}	2.9 ± 0.5 x 10^{-4}

Table 2: Characteristic values, slope in capillary and draining regime and E (m^3 s^{-1}) and D ($m^{1/3}$ $s^{2/3}$) extracted from the curve thickness versus the withdrawal speed curve (log/log

scale).

The slopes in these two regimes were determined and are displayed in table 2. These slopes are consistent with the semi-experimental expression of the thickness (h_f) versus the withdrawal speed (U_0) which, in the case of a dried film formed upon solvent evaporation, can be written as follows (equation 1).[19]

$$h_f = k_i \left(\frac{E}{L}\frac{1}{U_0} + D\,U_0^{2/3}\right) \qquad \text{Eq. (1)}$$

where k_i depends on the mass concentration of the polymer in the suspension (c_i in g cm^{-3}) and the density of the polymer (ρ_i in g cm^{-3}) by $k_i = c_i/\rho_i$. E, L, D are the evaporation rate, the film width and the global draining constant respectively (in our case, k_i varies from 4.3 x 10^{-2} and 4.7 x 10^{-2} and L was 0.01 m).

As shown in this expression, the evolution of the thickness with the withdrawal speed makes it possible to distinguish between a first regime known as the capillary regime observed at low withdrawal speed, where thickness is proportional to the inverse of the speed, and a second draining regime at high withdrawal speed, where thickness is proportional to the withdrawal speed to the power 2/3. The capillary regime is controlled by the capillarity feeding of the developing film as the solvent evaporates, resulting in thicker films as the withdrawal speed drops. In contrast, the draining regime is governed by an equilibrium between the suspension viscous drag and surface tension (described by the Landau-Levitch equation)[7] leading to greater film thicknesses beyond the critical speed.

An essential criterion for nanocomposite films (and thus their applications) is the amount of NPs in the film, their distribution in the volume and on the surface[29]. This leads to the following question: could the deposition regime (i.e. the withdrawal speed) affect the composition of the film and/or the distribution of the particles (i.e. the concentration of the NPs in the final film and on the surface)?

3- Quantification of the total number of NPs in the film.

To determine the total number of NPs in the nanocomposite film, different methods were used depending on the number of NPs in the film in order to achieve an accurate count.

- The A10 films were fractured in liquid nitrogen and the cross-sections were observed by SEM to examine the distribution of the particles over the sections. As shown in Figure 2a, the NPs are clearly visible and appear to be well spread over all the sections. No agglomeration was detected and as expected, the observed NPs retained their size (diameter of 26 nm) after deposition. This size stability was also verified by TEM imaging on a nanocomposite film dip-coated onto a TEM grid attached to a substrate (see Figure SI-3b). The NPs of the A10 films were counted on the SEM cross-sections and these counts were converted to numbers of NPs in the whole thickness of the film for a basal surface of 1µm² taking an estimated SEM information depth of 25 nm. Indeed, in SEM, images result from the secondary electrons and backscattered electrons escaping from the near layer whose thickness depends on the energy of primary electrons (15 keV) and the nature of the material (here an insulating layer). According to Butler[33], for backscattered electrons in such a material at this energy, the probed thickness is estimated at 25 nm.

- The A1 and A5 films were calcined in order to leave on the surface of the substrate only the NPs, as the PVP was calcined. AFM imaging of calcined films was carried out. Figure 2b shows a typical AFM image for an A5 film (other images are displayed in Figure SI-4) where the NPs can be clearly seen on the images and counted. It should be mentioned that the particle aggregation observed after calcination does not reflect the actual situation in the polymer nanocomposite since the degradation of the polymer is accompanied by a reorganization of the NP network.

Two different methods were used because on the one hand, examination of the cross-sections in SEM is not an appropriate method for A1 and A5 since the numbers counted are not high enough and on the other hand, counting after calcination is not valid for A10 since in this case there are too many NPs to be counted in the calcined films and NPs can be superposed.

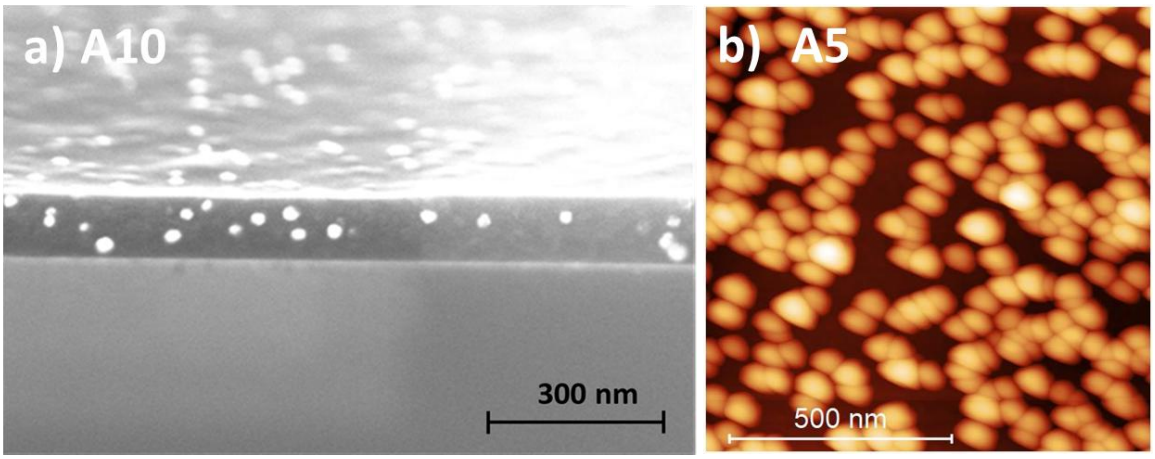

Figure 2: Examples of a) SEM cross-section image of an A10 film and b) AFM image of an A5 film after calcination.

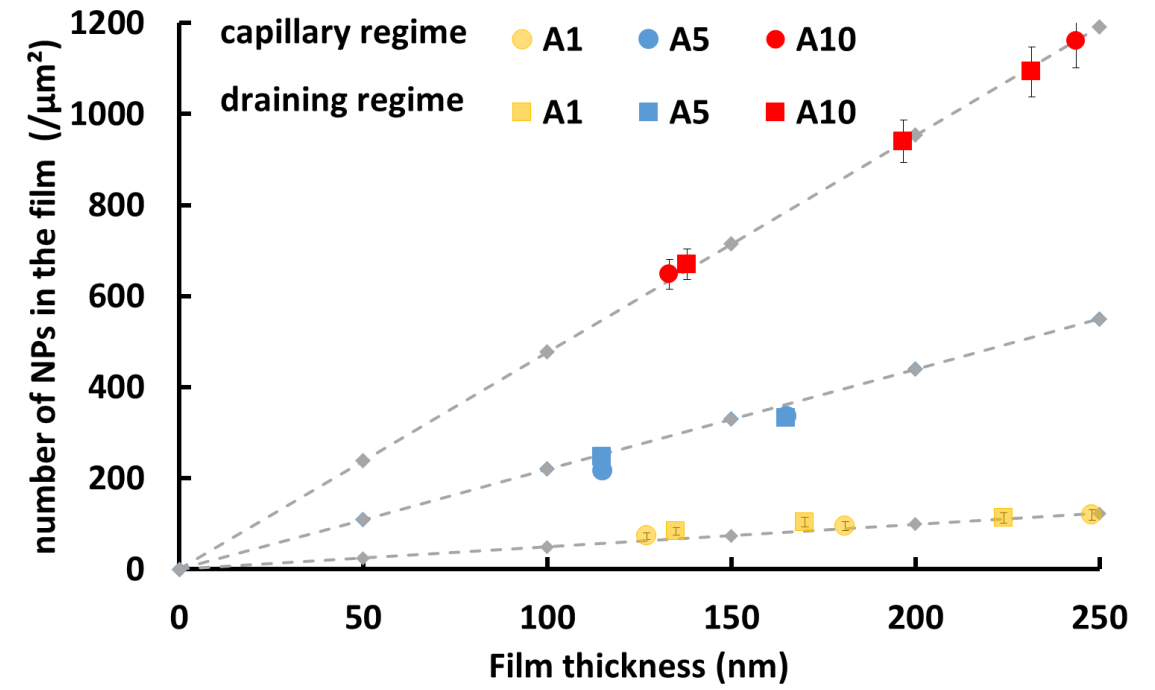

Figure 3: Number of NPs counted as a function of film thickness for A1, A5 (calcination and AFM counting) and A10 (examination of the cross-section by SEM) in the deposition draining (square) and capillary (circle) regimes. The grey symbols represent the calculated numbers of NPs for film thicknesses of 50, 100, 150, 200 and 250 nm. The grey dotted lines are drawn to guide the eyes. The relative standard deviation is estimated to be around 10%.

Figure 3 summarizes the number of NPs counted per surface area, for thin films with an A1, A5 and A10 composition as a function of the film thickness. As expected, the experimental

number of NPs increases with the film thickness and NP concentration. Interestingly, the regime does not seem to have a significant influence on the number of particles dragged during withdrawal. These experimental data were compared to the calculated numbers of NPs (see SI-5). The grey lines in Figure 3 represent the calculated numbers of NPs in the films assuming that there is no preferential drag of one component (PVP or NPs). As the experimental points follow this line, this hypothesis is verified, given the precision of the measurement. In order to understand such behavior, it is important to bear in mind that, due to the small amount of solid content in the suspension (e.g. 3.8 % for A5), the liquid film dragged before evaporation (in the draining regime) is much thicker than the residual solid film. As an illustration, a dry film with a thickness of 100 nm results from a liquid film of 2.6 µm. In these conditions, the diameter of the NPs (26 nm) is small in comparison to the thickness of the liquid film at the stagnation point[1] (the position where the suspension is dragged by the substrate). As shown by several authors [9, 10, 12] in the draining regime, particle entrainment in a liquid is hindered if the particles are trapped in the meniscus, which happens when the diameter of the particles is higher than the thickness at the stagnation point. As demonstrated above, the particles are too small to be trapped in the meniscus, confirming the absence of preferential drag.

In the capillary regime, the situation is different since the deposition is driven by a capillary flow triggered by the evaporation of the solvent from the edge of the meniscus. In this case, the film is built by the accumulation of solid materials near the contact line (in contrast to the situation in the draining regime where a liquid film is dragged and dried afterwards). However, this difference in mechanism does not affect the NP deposition and, again, the small size of the NPs in comparison to the dimension of the liquid meniscus can account for such behavior.

We can conclude from this first section that the concentration of NPs in the dried film is consistent with the composition of the deposited suspension, with no specific entrainment of the components. In the next section, we examine more closely the distribution of the NPs within the film in order to investigate the potential existence of a depletion or segregation of the NPs at the surface. For that purpose, the surface of the films was examined by AFM and SEM.

4- Observation by AFM and SEM of the film surface

- *AFM imaging*

Figure 4 illustrates the surface topographies of A0, A1, A5, and A10 thin films for two different withdrawal speeds leading to the same thickness of 250 nm, one belonging to the capillary regime and the other to the draining regime. Regardless of the withdrawal speed, the surface of the neat PVP film remained completely smooth. As a result, the NPs in the near surface area are clearly visible as revealed by dots (circular bumps) in the images of the nanocomposite films, both for the capillary and the draining regimes. From Figure 4, it can be seen that the NPs are quite well spread over the whole area with however a tendency to form small aggregates. A statistical analysis of the dimension of these bumps was carried out, showing a moderate height (maximum of 4 nm height) and a diameter (more than 50 nm) greater than the particle size itself (26 nm) as shown in Figure SI-6 for typical AFM height cross-sections. It is worth noting that with this height, the increase in the bump diameter due to the tip convolution effect is limited (less than 15 nm). The observation of bumps with a diameter larger than 50 nm is consequently not in favor of naked particles emerging from the surface, but is strong evidence of the existence of a polymer layer covering the nanoparticle, leading to a higher apparent diameter. In fact, a particle in the near surface layer induces a surface deformation, manifested as a topographic prominence in AFM, whose amplitude depends on the particle depth. The results of the DLS analysis of the suspension A10 (Figure SI-2) showing a greater diameter of NPs is consistent with the encapsulation of the particles with the PVP. Considering the limited surface deformation amplitude observed in the images (maximum of 4 nm height), it can be concluded that only the particles in the near surface layer can be observed (see below for an estimation of the "depth of information").

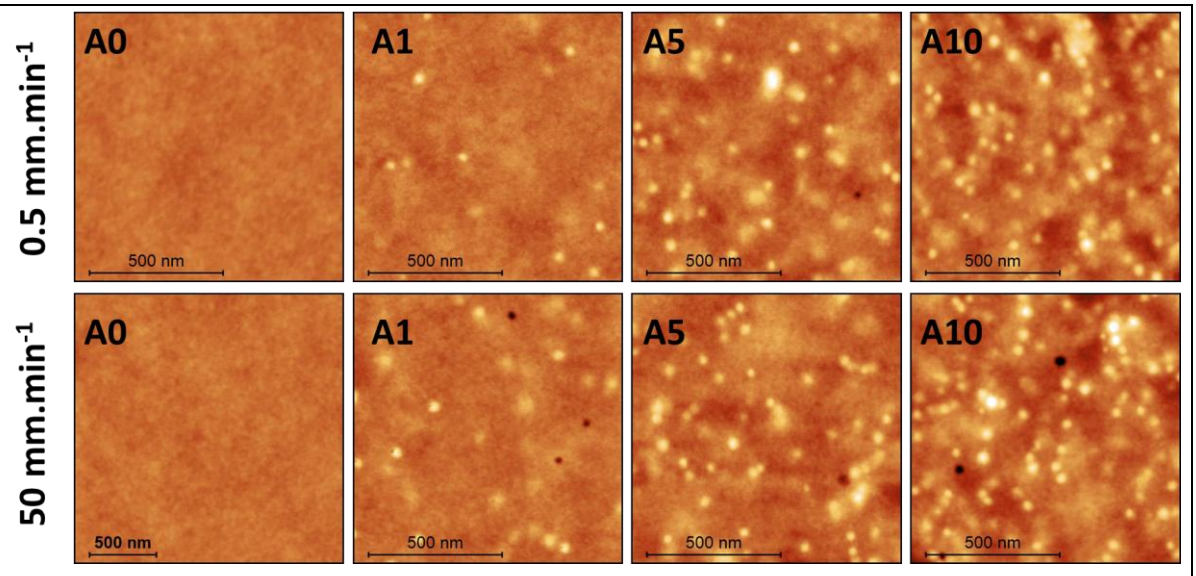

Figure 4: AFM images of films obtained for solution A0 and suspensions A1, A5 and A10 at

withdrawal speeds of 0.5 (film thickness: 240 nm) and 50 mm min^{-1} (film thickness: 212 nm). (z scale is 10 nm)

In order to investigate the number of NPs on the surface, AFM analysis of the nanocomposite thin films was carried out. The counting was based on the relative topographic prominence induced by the presence of the NPs. The particles were first counted manually and the counting was rationalized by using image analysis software. For this purpose, the particles inducing a relative topographic prominence higher than an arbitrary prominence threshold value (1.5 nm) were counted and summed as N_{AFM}. Other threshold values were tested (Figure SI-7a) and led to the same conclusion, as shown in Figure SI-7b.

The number of NPs N_{AFM} detected by AFM for the whole range of withdrawal speeds (0.3 - 130 mm min^{-1}) is presented in Figure 5 for the A10 composition. This figure enables the influence of the NPs detected in the draining (square) and the capillary (circle) regimes to be compared. For a better comparison, samples of similar thickness were targeted in the two regimes (for example, the thickness 375 nm was achieved in both the draining and the capillary regime, at withdrawal speeds of respectively 130 and 0.3 mm min^{-1}). Whereas similar numbers of NPs are detected for the thicker films in the two regimes (thickness > 200 nm), this figure clearly shows an opposite trend as the films become thinner. More NPs are detected at the surface of the film in the draining regime, with an increased number of NPs as the film thickness decreases. The results obtained for A1 and A5 are presented in Figure SI-7b and confirm these tendencies. A Student t test confirmed that the values obtained at low thicknesses in the draining regime were significantly different from the values monitored in the capillary regime for the same range of thickness (p values < 0.05).

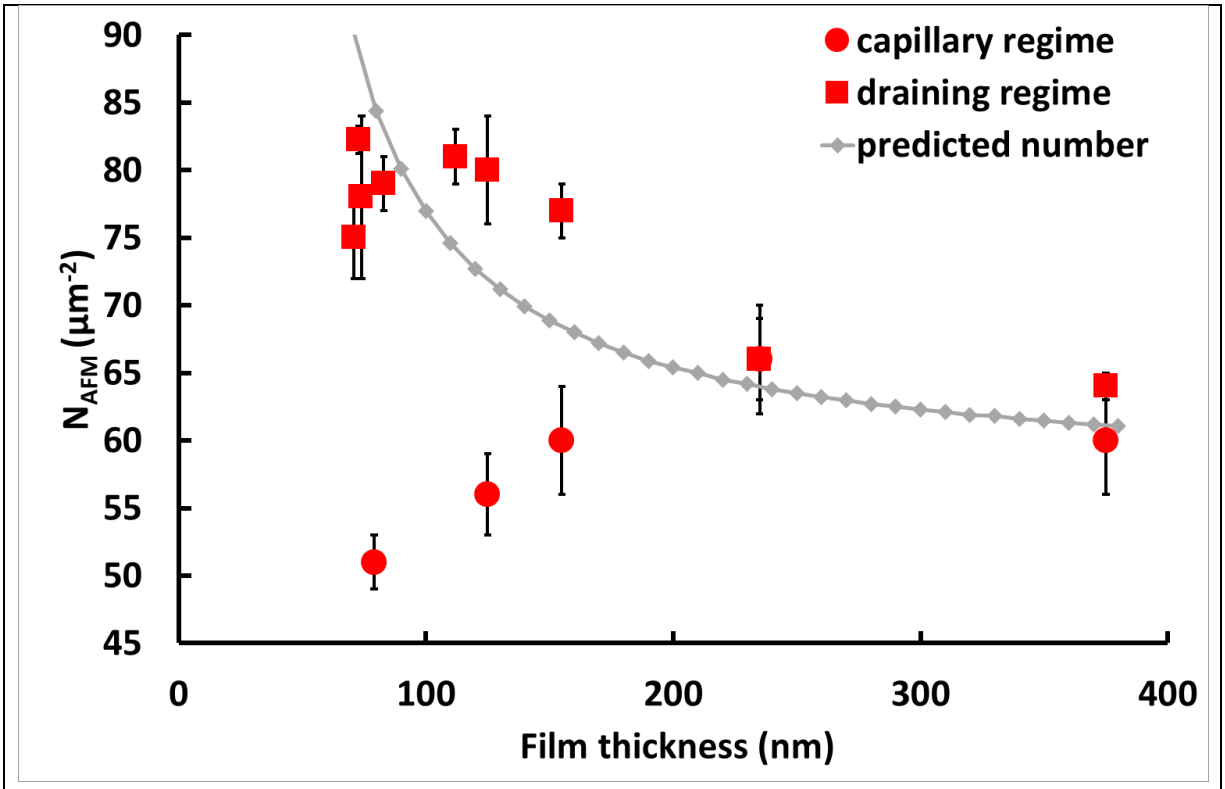

Figure 5: Number of NPs counted by AFM (NAFM) as a function of the film thickness for the A10 composition, in the draining (square) and capillary (circle) regimes. The grey symbols represent the predicted numbers of NPs for different thicknesses between 70 and 380 nm. The experimental standard deviations are taken as errors bars and calculated for each point.

- *SEM imaging*

SEM imaging was performed on A10 films to confirm the AFM results. Figure 6 presents typical SEM images of the surface of an A10 film (125 nm thick) in capillary and in draining regimes. The particles can be observed as gray spots due to the chemical contrast between the particles (silica) and the matrix (polymer). Each particle displays a gray level that is related to the depth of the particles: brighter spots correspond to the particles closest to the surface while the less bright ones are caused by the deeper particles. These SEM images are not composed only of secondary electrons (coming from at most 2 nm) but also from backscattered electrons coming from deeper levels and which lead to a higher information depth estimated at 25 nm for polymer.[Erreur ! Signet non défini.]

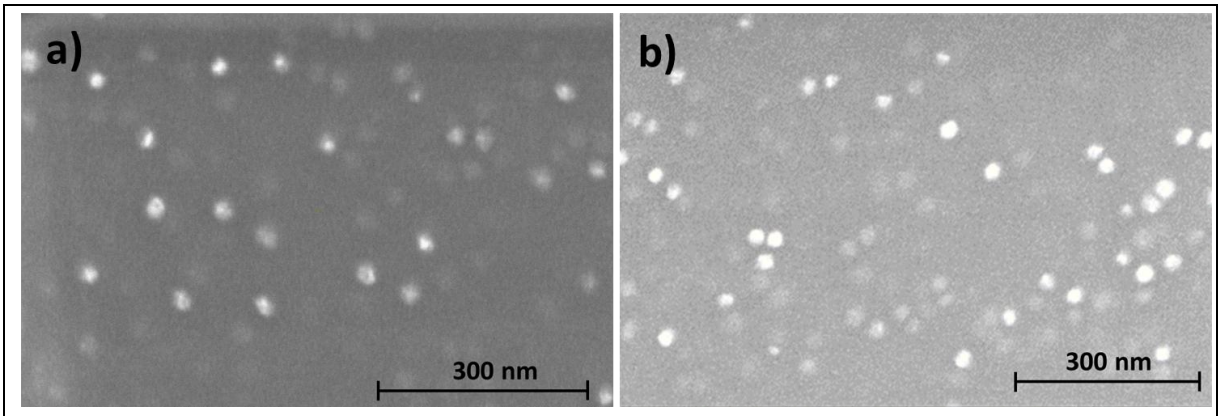

Figure 6: SEM images collected for the A10 film, 125 nm thick. Top view images for capillary (a) and for the draining (b) regimes.

Image processing was performed to distinguish and count the particles NPs. Similarly to the AFM approach, an arbitrary gray-level threshold value was chosen to reflect particles depth limit. This led to the number N_{SEM}. An example of image processing is given in the supporting information (SI-8). For a given sample, the numbers of NPs obtained by AFM (N_{AFM}) and SEM (N_{SEM}) were different due to the difference of information depth and the selection of arbitrary threshold values. As an example, N_{AFM} was 77 NPs μm^{-2} whereas N_{SEM} was 131 NPs μm^{-2} for an A10 film at a thickness of 155 nm. The difference between these numbers results from the probes (AFM tip and electron beam), the probed properties (topography and electron emission) and consequently information depths, that are different. These numbers cannot therefore be directly compared. However, using a given type of counting allows for the study of the impact of the deposition conditions on the number of NPs on the surface.

Figure 7 displays N_{SEM} of samples having similar thicknesses (~ 115 and 155 nm), but obtained in the capillary (open red circles) and in the draining (open red squares) regimes. The observation confirms a higher number of NPs in the draining regime, with a more pronounced effect for the thinner films, similarly to the AFM observations. The results obtained for N_{AFM} are also reported on figure 7 (full red squares and circles) confirming that even if the N_{AFM} and N_{SEM} numbers are not the same, they show the same trend: the number of NPs at the surface is lower for the capillary regime than for the draining regime and this difference is exacerbated for the lowest thickness.

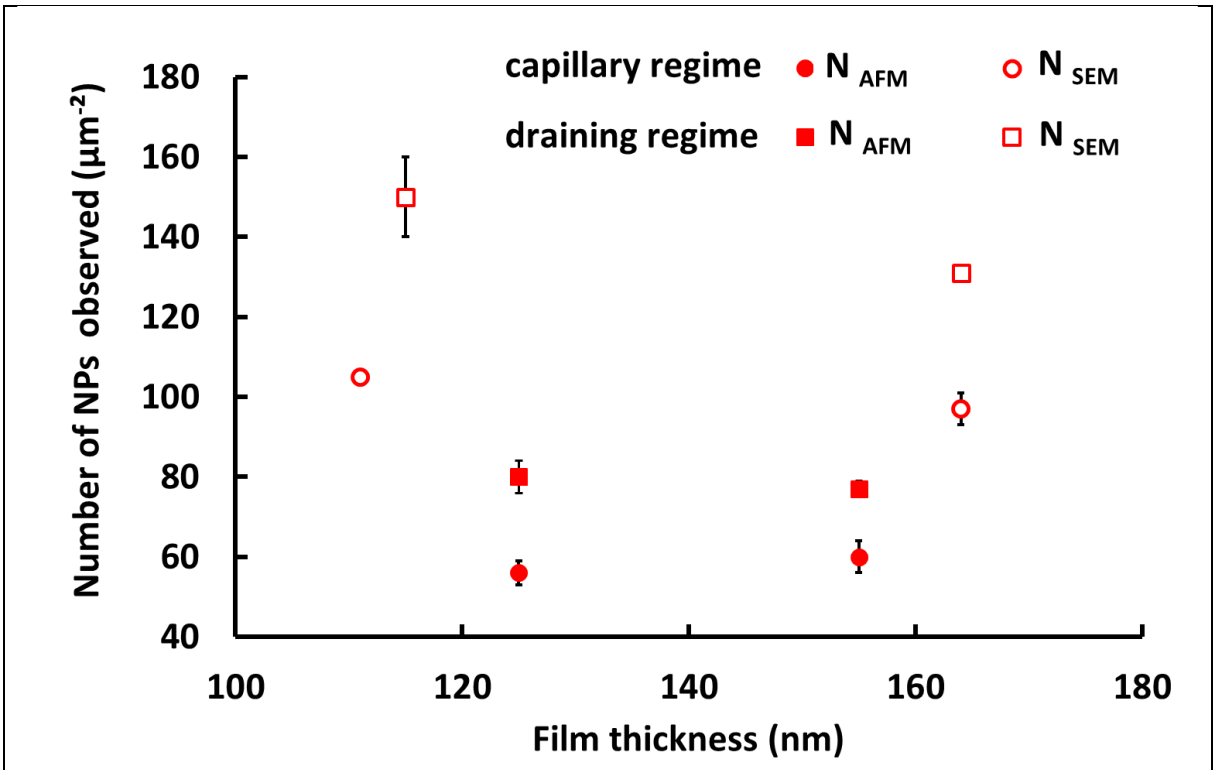

Figure 7: number of NPs counted from the SEM (N_{SEM}) (open symbols) and the AFM images (N_{AFM}) (full symbols) for the A10 composition, as a function of the thickness and the deposition regime (draining (squares) or capillary (circles)). In this figure, the experimental standard deviations are taken as errors bars.

- *Comparison between predicted NP numbers and experimental observations*

In order to compare the experimental number of NPs, evaluated by AFM and by SEM, to the number of particles in a homogeneous film, we need to predict the number of NPs in the near surface layer of the nanocomposite film. The evaluation of the thickness of the layer probed in AFM and SEM is thus an important question. We have shown that both AFM and SEM were able to detect buried particles: in AFM because the particles can provoke a deformation of the surface and in SEM, because backscattered electrons emitted from the NPs can travel through a thin polymer layer. Of course, these phenomena are only valid within a given surface layer thickness, and vanish as the NPs move away from the surface.

In AFM, the estimation of the probed thickness layer (8-12 nm) was based on the analysis of the surface topography as described in the supporting information (see SI-9). Outside this layer (i.e. for NPs below 8-12 nm), NPs do not provoke any surface deformation and thus are not detected in AFM. In SEM, images result from the secondary electrons and backscattered electrons escaping from the near layer whose thickness depends on the nature of the material (here an insulating layer). As already explained above, the escape depth for backscattered

electrons in such material at 15 keV is estimated to be 25 nm. Since the information depth is larger in SEM (25 nm) than in AFM (8-12nm), the number of NPs counted in SEM is larger than in AFM, confirming the results obtained earlier.

Having the thickness of the probed layer, we are now able to predict the number of particles present in a surface layer ($N_{NP\text{-}surf}$) as described in the supporting information. In brief, this number (per surface area) can be calculated by multiplying the total number of particles in the film (per surface area) by the ratio of the thickness of the probed layer / film thickness (see SI-9). Figure 5 displays such a calculation for the AFM counting: as the thickness decreases, the calculated number of NPs (grey line) increases due to the fact that the particles cannot enter an exclusion zone at the interfaces. This leads us to consider h-2R instead of h in eq. 4 in SI-9, leading to an increase of $N_{NP\text{-}surf}$ when h decreases.

These calculations fit quite well with the experimental data obtained in the draining regime, even in the case of the thinner samples ($N_{NP\text{-}surf}$ increases), confirming the validity of the approach. Since the experimental numbers of NPs counted in AFM match with calculated values, one can conclude that the NP/polymer ratio is preserved, indicating that no preferential entrainment of one of the two components takes place at the surface.

The behavior in the capillary regime is completely different: the calculated numbers of NPs fit the experimental values only at high thicknesses and strongly deviate at low thicknesses (with a number of NPs in the near surface layer lower than expected). These results show an unexpected discontinuity of the number of NPs in the near surface layer at the critical speed (corresponding to a minimal thickness of ca. 80 nm), when the deposition shifts from the draining to the capillary regime. The NP depletion at the surface, obtained in the capillary regime at low thickness, suggests that together with the withdrawal speed, the thickness of the film and the deposition regime drive the number of NPs in the near surface layer. As this was not observed in the pure capillary and draining regimes, it may be the result of competition between all the phenomena (viscous drag, capillary force, evaporation and convective flow) that take place during dip-coating and are withdrawal speed dependent phenomena.

This unexpected result concerning the number of NPs in the surface layer has not been the subject of investigation so far, nor has it been reported by other publications, and now requires further investigations and simulations.

Conclusion

Thin films resulting from the dip-coating of suspensions of PVP/Ludox NPs were examined. The thicknesses of the films follow the classical additive law of an evaporative regime (with a slope -1) and a draining regime (with a slope 2/3 in a log-log scale). In the range of NP concentration examined in this study, no modification of the film thickness was reported in comparison to a neat PVP.

The films were examined using AFM and SEM. SEM cross-section imaging of the films and AFM imaging of calcinated film showed that the concentration of dragged particles was consistent with the concentration in the suspension. No influence of the deposition regime (or, if present, the influence is below the uncertainty of our results) was observed on the global NP concentration. In the draining regime, this is consistent with the literature results, which demonstrate that the particles used (26 nm) are too small to be trapped in the meniscus. A similar conclusion was drawn in the present study for the capillary regime.

The concentration of NPs at the surface was specifically examined. Counting of particles was performed on AFM and SEM images. Pure capillary and draining regimes lead to a number of particles that is consistent with a homogeneous distribution of the particles in the film. In between these two regimes (i.e. in a range of speeds which leads to lower thicknesses and where the constitution of the film does not result from a pure regime), the numbers of particles observed on the surface do not lead to the same conclusion. In the draining branch, the NPs followed the theoretical calculation predicting an increased number of NPs as the thickness decreases, due to the presence of an exclusion zone at the interfaces. Unexpectedly, a NP depletion was observed in the capillary branch of the process, which could be the result of competition and interplay between time-dependent phenomena that take place during the dip-coating. To our knowledge, this phenomenon has not been previously reported and requires further investigations and simulations. This behavior will need to be carefully considered when preparing nanocomposite thin films where surface properties such as roughness or wettability need to be considered.

Acknowledgment:

The authors would like to thank the Region Centre Val de Loire for financial support of the ARD CVL MATEX program through a post-doctoral fellowship.

The authors would like to acknowledge Marjorie Roulet for TGA measurement, Samuel Guillot for DLS measurements and discussions, Fabienne Warmont for TEM imaging, Patrice Porion and Joel Puibasset for fruitful discussions.

References

[1] C. J. Brinker, A. J. Hurd, G. C. Frye, P. R. Schunk, C. S. Ashley, Sol-Gel Thin Film Formation, J. Ceram. Soc. Japan, (1991), 99, 862-877 https://doi.org/10.2109/jcersj.99.862

[2] D. Grosso, How to exploit the full potential of the dip-coating process to better control film formation, J. Mater. Chem.,(2011), 21, 17033−17038 https://doi.org/10.1039/C1JM12837J

[3] X. Tang, X. Yan, Dip-coating for fibrous materials: mechanism, methods and applications J Sol-Gel Sci. Technol., (2017), 81, 378–404, https://doi.org/10.1007/s10971-016-4197-7

[4] D. Quéré, Fluid coating on a fiber, Annu. Rev. Fluid Mech., (1999), 31, 347–384. https://doi.org/10.1146/annurev.fluid.31.1.347

[5] A. A. Raffi, M. A. Rahman, M. A. M. Salim, N. J. Ismail, M. H. D. Othman, A. F. Ismail, H. Bakhtiar, Surface treatment on polymeric polymethyl methacrylate (PMMA) core via dip-coating photopolymerisation curing method, Optical Fiber Technology (2020),57, 102215, https://doi.org/10.1016/j.yofte.2020.102215

[6] S. Kwon, W. Kim , H. Kim , S. Choi , B.-C. Park, S.-H. Kang, and K. C. Choi, Light-Emitting Devices: High Luminance Fiber-Based Polymer Light-Emitting Devices by a Dip-Coating Method, Adv. Electron. Mater. (2015), 1, 1500103 https://doi.org/10.1002/aelm.201570032

[7] L. Landau and B. Levich, "Dragging of a liquid by a moving plate," Acta Physico Chimica R.U.S.S., (1942), 17, 42-54.

[8] L. Champougny, B. Scheid, A. A. Korobkin and J. Rodríguez-Rodríguez, Dip-coating flow in the presence of two immiscible liquids, J. Fluid Mech. (2021), 922, A26, https://doi.org/10.1017/jfm.2021.541

[9] B.M. Dincau, M.Z. Bazant, E. Dressaire, and A. Sauret, Capillary Sorting of Particles by Dip Coating, Phys. Rev. Applied (2019),12, 011001

[10] A. Sauret, A. Gans, B. Colnet, G. Saingier, M. Z. Bazant and E. Dressaire, Capillary filtering of particles during dip coating, Phys. Rev. Fluids. (2019), 4, 054303 https://doi.org/10.1103/PhysRevFluids.4.054303

[11] D.-H. Jeong, M. K. H. Lee, V. Thiévenaz, M. Z. Bazant and A. Sauret, Dip coating of bidisperse particulate suspensions. J. Fluid Mech., (2022), 936, A36. https://doi.org/10.1017/jfm.2022.79

[12] S. Palma and H. Lhuissier, Dip-coating with a particulate suspension, J. Fluid Mech. (2019), 869, R3, https://doi.org/10.1017/jfm.2019.267

[13] C. E. Colosqui, J. F. Morris, and H. A. Stone, Hydrodynamically driven colloidal assembly in Dip Coating, Phys. Rev. Lett. (2013), 110, 188302 https://doi.org/10.1103/PhysRevLett.110.188302

[14] B. G. Jung, S.-H. Min, C.-W. Kwon, S.-H. Park, K.-B. Kim, and T.-S.Yoon, Colloidal Nanoparticle-Layer Formation Through Dip-Coating: Effect of Solvents and Substrate Withdrawing Speed, Journal of The Electrochemical Society, (2009), 156, K86-K90 https://doi.org/10.1149/1.3089364

[15] D. Qu, E. Ramé, and S. Garoff, Dip-coated films of volatile liquids, Physics of Fluids, (2002) 14, 1154 http://dx.doi.org/10.1063/1.1449467

[16] G. Berteloot, A. Daerr, F. Lequeux and L. Limat, Dip coating with colloids and evaporation Chemical Engineering and Processing / Process Intensification (2013), 68, 69–73. https://dx.doi.org/10.1016/j.cep.2012.09.001

[17] L. Malaquin, T. Kraus, H. Schmid, E. Delamarche, and H. Wolf, Controlled Particle Placement through Convective and Capillary Assembly, Langmuir (2007), 23, 11513-11521, http://dx.doi.org/10.1021/la700852c

[18] D. Nagao, R. Kameyama, H. Matsumoto, Y. Kobayashi , M. Konno, Single- and multi-layered patterns of polystyrene and silica particles assembled with a simple dip-coating Colloids and Surfaces A: Physicochem. Eng. Aspects 317 (2008) 722–729 http://dx.doi.org/10.1016/j.colsurfa.2007.12.011

[19] M. Faustini, B. Louis, P. A. Albouy, M. Kuemmel and D. Grosso, Preparation of Sol−Gel Films by Dip-Coating in Extreme Conditions, J. Phys. Chem. C, (2010), 114, 7637-7645 . https://doi.org/10.1021/jp9114755

[20] S. Roland, C. G. Gamys, J. Grosrenaud, S. Boissé, C. Pellerin, R.E. Prud'homme and C. G. Bazuin, Solvent Influence on Thickness, Composition, and Morphology Variation with Dip-Coating Rate in Supramolecular PS-b-P4VP Thin Films, Macromolecules, (2015), 48, 4823-4834. https://pubs.acs.org/doi/abs/10.1021/acs.macromol.5b00847

[21] S. Roland, R. E. Prud'homme and C.G. Bazuin, Morphology, Thickness, and Composition Evolution in Supramolecular Block Copolymer Films over a Wide Range of Dip-Coating Rates, ACS Macro Lett. (2012), 1, 973-976. https://pubs.acs.org/doi/full/10.1021/mz3003165

[22] A. Vital, M. Vayer, T. Tillocher, R. Dussart, M. Boufnichel and C. Sinturel, Morphology control in thin films of PS:PLA homopolymer blends by dip-coating deposition, Appl. Surf. Sci., (2017), 393, 127-133. https://doi.org/10.1016/j.apsusc.2016.09.151

[23] C. Sinturel, M. Vayer, F. Mahut, F. Bonnier, I. Chourpa and E. Munnier, Influence of PLGA nanoparticles on the deposition of model water-soluble biocompatible polymers by dip coating, Colloids and Surfaces A (2021), 608, 125591, https://doi.org/10.1016/j.colsurfa.2020.125591

[24] K.Wang, R. K. Bordia, L. N. Brush, A semi-empirical power-law model for the dip-coating of a substrate into a particle-containing, non-Newtonian, complex fluid system, Ceramics International 45 (2019) 6655–6664, https://doi.org/10.1016/j.ceramint.2018.12.154

[25] M. Vayer, A. Pineau, F. Warmont, M. Roulet and C. Sinturel, Constrained crystallization of poly(L-lactic acid) in thin films prepared by dip coating, Eur. Polym. J., (2018), 101, 332-340. https://doi.org/10.1016/j.eurpolymj.2018.03.006

[26] M. Sabapathy, S. D. C. Pushpam, M. G. Basavaraj, and E. Mani, Synthesis of Single and Multipatch Particles by Dip-Coating Method and Self-Assembly Thereof, Langmuir, (2015), 31, 1255−1261. https://doi.org/10.1021/la503531a

[27] X. Liu, S. Veldhuis, R. Mathews, I. Zhitomirsky, Dip coating of poly(ethyl methacrylate) and composites from solutions in isopropanol-water co-solvent Colloids and Surfaces A: Physicochemical and Engineering Aspects (2021), 631, 127703 https://doi.org/10.1016/j.colsurfa.2021.127703

[28] H. Uchiyama , R. Sasaki, H. Kozuka Evaporation-driven self-organization ophotoluminescent organic dye-doped silica-poly(vinylpyrrolidone) hybrid films prepared by low-speed dip-coating, Colloids and Surfaces A: Physicochem. Eng. Aspects(2014), 453, 1–6 http://dx.doi.org/10.1016/j.colsurfa.2014.03.066

[29] S. K. Kumar, V. Ganesan and R.A. Riggleman Perspective: Outstanding theoretical questions in polymer-nanoparticle hybrids, J. Chem. Phys. (2017), 147, 020901 https://doi.org/10.1063/1.4990501

[30] J. Kao, K. Thorkelsson, P. Bai, B. J. Rancatore and T. Xu Toward functional nanocomposites: taking the best of nanoparticles, polymers, and small molecules, Chem. Soc. Rev., 2013, 42, 2654-2678 https://doi.org/10.1039/C2CS35375J

[31] I.M. Alibe, K.A. Matori, H.A.A. Sidek, Y. Yaakob, U. Rashid, A. M. Alibe, M. H. M. Zaid, S. Nasir, M. M. Nasir, Effects of polyvinylpyrrolidone on structural and optical properties of willemite semiconductor nanoparticles by polymer thermal treatment method. J Therm Anal Calorim (2019) 136, 2249–2268 https://doi.org/10.1007/s10973-018-7874-7

[32] K. M. Koczkur, S. Mourdikoudis, L. Polavarapu, S. E. Skrabalak, Polyvinylpyrrolidone (PVP) in nanoparticle synthesis. *Dalton transactions*, (2015). *44*, 17883-17905.

[33] J. H. Butler, D. C. Joy, G. F. Bradley S. J. Krause , Low-voltage scanning electron microscopy of polymers, Polym (1995) 36, 1781-1790.